Mon. Not. R. astr. Soc. (1985) **213,** 451–471

Evolution of barred galaxies by dynamical friction

Martin D. Weinberg★ *Department of Physics, Center for Theoretical Physics, and Center for Space Research, Massachusetts Institute of Technology, Cambridge, Massachusetts 02139, USA*

Accepted 1984 November 6. Received 1984 November 6; in original form 1984 July 6

Summary. The transfer of angular momentum between the bar and halo components of a galaxy is computed using both analytic dynamical friction theory and 'semi-restricted' *n*-body simulations. The two methods yield results which are in qualitative agreement and demonstrate that dynamical friction can exert strong torques on galactic bars. A rotating rigid bar with typical parameters initially ending at corotation slows down in several bar rotation times in the presence of an isothermal halo. This rapid angular momentum transfer implies that the corotation radius must be far beyond the end of the bar unless: (1) angular momentum is added to the bar (i.e. by the disc) allowing an equilibrium bar pattern speed to be reached; (2) the galactic halo is small or non-existent; or (3) the bar is weak.

1 Introduction

Approximately one third of all disc galaxies are barred (Sandage & Tammann 1981). Bars also appear naturally as the dominant unstable modes in numerical simulations of disc-like stellar systems (e.g. Miller 1978; Miller & Smith 1979). In light of their ubiquity, it is important to understand the role of bars in galactic evolution. In this paper, I investigate the long-term angular momentum transfer between the bar and the halo. Throughout this paper, the term 'halo' denotes any collisionless, approximately spherically distributed mass including the bulge and spheroidal components and any unseen extended halo. I shall concentrate on the bar–halo interaction although the bar–disc interaction is briefly discussed in Section 3.4. Mark (1976) describes the long-term angular momentum transfer from the disc to the halo due to spiral structure.

Much of the previous work on bars in haloes has focused on the stability of disc to forming bars. This work followed a suggestion by Ostriker & Peebles (1973) that a massive halo can suppress bar formation. Since the purpose of these investigations was to determine the stability of the disc, in most cases fixed haloes were used (Hohl 1976; Sellwood 1981; Combes & Sanders 1981). In the investigations that used live haloes (e.g. Hohl 1978), the integration was terminated as soon as the bar reached an equilibrium configuration. The sole exception is a paper by Sellwood (1980) who

★Present address: Space Sciences Building, Cornell University, Ithaca, NY 14853, USA.

followed a disc+live halo model for approximately one rotation period after a strong bar formed. He found that after a strong bar formed, the bulge began to gain angular momentum from the disc. This result was an important clue that the interaction between the halo and the bar may have interesting long-term consequences. The result suggests that the halo may exert a drag on the bar just as a homogeneous medium exerts a drag on a test mass in the standard picture of dynamical friction (Chandrasekhar 1943). In fact, there is observational evidence due to Kormendy (1982) that bulges of barred galaxies rotate more rapidly than those of unbarred galaxies although the scenario suggested by Kormendy is more complicated than the picture developed here.

In order to obtain a better understanding of how dynamical friction leads to angular momentum transfer between the bar and the halo, I now present a simple example which illustrates the basic features of the more detailed models in the following sections. The drag on a test mass moving through an infinite homogeneous medium may be interpreted as the gravitational force of the wake excited by the test mass (e.g. Kalnajs 1972). This force is given by (Chandrasekhar 1943):

$$\frac{dv}{dt}=-\frac{4\pi G^2 m}{v^2}\ln\Lambda\varrho(<v) \tag{1}$$

where m is the mass of the test particle, $\varrho(<v)$ is the density of the background stars with speeds less than v, $\Lambda=b_{\max}/b_{\min}$ where $b_{\max}$ and $b_{\min}$ are the maximum and minimum impact parameters. Usually $b_{\min}\approx Gm/v^2$, the impact parameter for a large deflection, and $b_{\max}$ is the scale size of the background. Now, consider a schematic model for a bar consisting of two point masses, m, at the ends of a rigid rod of length $2d$ rotating about its midpoint with an angular velocity or pattern speed, Ω_b. The 'bar' is placed at the centre of a spherical distribution of stars which represents the halo component of the galaxy. Ignoring the curvature of the trajectories of the masses and any interaction between the wakes of the two masses, and treating the halo as a locally homogeneous medium, the torque on the bar follows from equation (1):

$$\frac{dJ_b}{dt}=2md\frac{dv}{dt}=-\frac{8\pi G^2 m^2 d}{v^2}\ln\Lambda\varrho(<v), \tag{2}$$

where the angular momentum J_b of the bar is $J_b=2md^2\Omega_b$ and $v=\Omega_b d$. For simplicity, let the halo be a singular isothermal sphere with velocity dispersion σ and density $\varrho(r)=\sigma^2/(2\pi Gr^2)$. The velocity distribution of stars in an isothermal sphere is Maxwellian so that $\varrho(<v)=\varrho(d)[\Phi(v/\sqrt{2}\sigma)-v/\sqrt{2}\sigma\Phi'(v/\sqrt{2}\sigma)]$ where Φ is the error function. It is convenient to define the 'corotation parameter,' S, as the ratio of the velocity at the end of the bar to the circular velocity of a star at the same radius. In this case, $S=\Omega_b d/\sqrt{2}\sigma$. Equation (2) then becomes

$$\frac{dJ_b}{dt}=2md^2\frac{\sqrt{2}\sigma}{d}\frac{dS}{dt}=-\frac{2Gm^2\ln\Lambda}{d}\frac{1}{S^2}[\Phi(S)-S\Phi'(S)]. \tag{3}$$

Defining T_0 to be the bar's initial rotation time for $S=1$ and letting f be the ratio of the mass of the bar $2m$ to the mass of the halo inside d, the time it takes for the angular velocity to decrease by a factor of two, the half-life, is given by:

$$\frac{T_{1/2}}{T_0}=\frac{1}{\pi f\ln\Lambda}\int_{1/2}^{1}\frac{S^2\,dS}{[\Phi(S)-S\Phi'(S)]}\simeq\frac{0.404}{f\ln\Lambda}. \tag{4}$$

The value of $\ln\Lambda$ is uncertain but it is generally of order unity or larger. Barred galaxies typically have comparable luminosities in the bar and bulge components inside the bar's major axis (Kormendy 1983, private communication). Assuming the same mass-to-light ratio for both

components gives $f\sim1$. This model therefore suggests that dynamical friction can slow a bar in a rotation time. However, the model is not realistic enough to be convincing by itself. In particular: (1) bars do not look like pairs of point masses and the standard dynamical friction theory can not be used to derive the torque from an extended bar model; (2) equation (1) results from the force on a test mass from an infinite homogeneous medium where the stars move on straight lines, while a real halo is spherical and inhomogeneous, and composed of stars moving on planar orbits. In Section 3, I use the analytic theory of dynamical friction for spherical systems (Tremaine & Weinberg 1984, hereafter Paper I) to compute the half-life using a bar model with the potential $U(r)Y_{2,2}(\theta,\phi)$. It will turn out that the bar half-life, $T_{1/2}$, is of order T_0, just as in the simple model presented above. However, this calculation still contains the following approximations: (1) the bar is assumed to be weak compared to the halo which is not the case in observed galaxies; and (2) the bar model only includes the $Y_{2,2}$ component. Thus, in Section 4, a semi-restricted n-body simulation (e.g. Lin & Tremaine 1983) is performed using an ellipsoidal bar model to check the dynamical friction theory. I conclude with Section 5.

In the next section, Section 2, the basic assumptions of this investigation are presented and discussed.

2 Basic assumptions

There are three basic assumptions that will be employed throughout this paper:

(1) The unperturbed halo component will be assumed to be a singular isothermal sphere. This isothermal sphere has the potential

$$U(r)=2\sigma^2\ln r/a_1 \tag{5}$$

where a_1 is an arbitrary scale length that will later be associated with the semi-major axis of the bar and σ is the velocity dispersion. The phase-space distribution function for the halo is $f=f_0\exp(-E/\sigma^2)$ where E is the energy of a given orbit. I will choose f_0 such that the mass inside the radius a_1 is unity:

$$M=\frac{2\sigma^2 a_1}{G}=1. \tag{6}$$

Using equation (6), f_0 is easily evaluated and the distribution function becomes:

$$f=\frac{1}{4\sqrt{2}\pi^{5/2}G\sigma a_1^2}\exp(-E/\sigma^2) \tag{7}$$

Unlike observed spheroidal components in some galaxies, the singular isothermal sphere does not rotate and does not have an intrinsic scale length. However, the simple structure of the isothermal sphere greatly simplifies the analytic treatment of Section 3 without, I believe, significantly limiting the results of the investigation.

(2) The bar is assumed to rotate as a rigid body about the z-axis so that the torque τ_z and the angular acceleration are related by

$$\tau_z=I\dot{\Omega}_b, \tag{8}$$

where I is the moment of inertia of the bar. More generally, we can write $\tau_z=I_{\rm eff}\dot{\Omega}_b$ where the effective moment of inertia $I_{\rm eff}$ changes as the bar evolves and may even be negative (e.g. Weinberg & Tremaine 1983). Since, in this paper, I am primarily interested in the magnitude of the angular momentum transfer rather than its effect on the structure of the bar, I take $I_{\rm eff}=I$ for simplicity.

(3) As discussed in Section 1, the torque on the bar results from the interaction between the bar and the wake it excites in the halo. A fully self-consistent treatment would have to include the self-gravity of the wake. White (1983) found that self-consistent simulations of galaxy mergers yielded orbital decay rates that differed only by a factor of two from the rates predicted by dynamical friction theory. Thus, I do not expect that the inclusion of self-gravity would qualitatively change the results obtained here although it would significantly complicate the analysis. In all of the calculations that follow, I will ignore the effects of the self-gravity of the wake.

3 Analytic treatment of bar slow-down

The object of this section is to use perturbation theory to estimate the torque exerted by a halo on a rotating bar. Instead of calculating the wake directly by solving the Poisson and Vlasov equations, it is easier to compute the torque on a single star and then sum over all the stars. Let the perturbation parameter, ε, be the ratio of the mass of the bar to the mass of the unperturbed stellar sphere inside the bar radius. Thus the bar potential is $O(\varepsilon)$ with respect to the unperturbed potential. We found in Paper I that the dominant angular momentum transfer occurs at resonances or commensurabilities between the radial and azimuthal frequencies of the stars and the pattern speed of the bar. In the limit that the bar pattern speed changes rapidly or the bar is weak, the perturbation to the stellar orbit is small and the net torque on the bar is $O(\varepsilon^2)$. In this case the torque is given by a generalization of a formula derived by Lynden-Bell & Kalnajs (1972). A brief derivation of the Lynden-Bell & Kalnajs (hereafter LBK) formula will be presented in Section 3.1 (see Paper I for additional details). If the bar pattern speed evolves slowly or the bar is strong, the non-linear character of the resonance may dominate. I call this regime the 'slow limit'. Torques in the slow limit are $O(\varepsilon^{3/2})$. I will discuss the possibility and consequencies of angular momentum transfer in this regime in Section 3.2. In Section 3.3 the torque formulae are evaluated numerically and the slow-down rates are computed for a family of models. Since the bar is actually imbedded in a disc which up to now has been ignored, one would also like to include the effects of disc torques on the bar. Thus in Section 3.4 I add a cold disc and discuss its evolutionary effect on the bar–halo system.

3.1 THE LYNDEN-BELL & KALNAJS FORMULA

First, consider the motion of a particle of unit mass in the unperturbed galaxy potential $U(r)$. The Hamiltonian is

$$H_0=\frac{1}{2}\left(p_1^2+\frac{p_2^2}{r^2}+\frac{p_3^2}{r^2\sin^2\theta}\right)+U(r), \tag{9}$$

where $(p_2, p_2, p_3)=(\dot{r}, r^2\dot{\theta}, r^2\sin^2\theta\,\dot{\phi})$ are the momenta conjugate to the spherical coordinates $(q_1, q_2, q_3)=(r, \theta, \phi)$. Since ϕ is ignorable in equation (9), p_3 is conserved and is equal to the z-component of angular momentum J_z.

The total angular momentum J and energy E are also conserved:

$$J=(p_2^2+p_3^2/\sin^2\theta)^{1/2}, \tag{10}$$

$$E=\frac{1}{2}\dot{r}^2+\frac{J^2}{2r^2}+U(r). \tag{11}$$

The energy equation (11) has real solutions for $\dot{r}$ only when $r_p<r<r_a$, where r_p and r_a, the periapse

and apoapse, satisfy $E=J^2/2r^2+U(r)$. The radial period, t_r (time from periapse to periapse), and radial frequency Ω_1 are given by

$$t_r=\frac{2\pi}{\Omega_1}=2\int_{r_p}^{r_a}\frac{dr}{[2(E-U)-J^2/r^2]^{1/2}}. \tag{12}$$

In one radial period the star advances by an angle in the plane of its orbit $\Delta\psi$, where $\Delta\psi=\Omega_2 t_r$ and

$$\frac{\Omega_2}{\Omega_1}=\frac{J}{\pi}\int_{r_p}^{r_a}\frac{dr}{r^2[2(E-U)-J^2/r^2]^{1/2}}. \tag{13}$$

The radial action is

$$I_r=\frac{1}{2\pi}\oint dr\,p_r=\frac{1}{\pi}\int_{r_p}^{r_a}dr\,[2(E-U)-J^2/r^2]^{1/2}. \tag{14}$$

Following the method developed in Paper I, I use the canonical variables $(I_1, I_2, I_3)=(I_r, J, J_z)$. The conjugate coordinates are the angles (w_1, w_2, w_3). The angle w_1 is given by

$$w_1=\Omega_1\int_{C_1}\frac{|dr|}{[2(E-U)-J^2/r^2]^{1/2}}. \tag{15}$$

The integration contour C_1 goes from periapse to the current position. The integrals are line integrals which increase monotonically along the orbit. It follows from equation (12) that w_1 is zero at periapse and increases by 2π in one radial period. The second angle variable is

$$w_2=\psi+\int_{C_1}|dr|[2(E-U)-J^2/r^2)]^{-1/2}(\Omega_2-J/r^2), \tag{16}$$

where

$$\psi=J\int_{C_2}|d\theta|[J^2-J_z^2/\sin^2\theta]^{-1/2}. \tag{17}$$

The integration contour C_2 starts at an ascending node (that is $\theta=\pi/2$, $\dot\theta<0$). We have shown that ψ is the angle from the ascending node to (r, θ, ϕ), measured in the orbit plane along the direction of orbital motion. The third angle variable w_3 is the azimuth of the ascending node.

Now, consider a bar with a pattern speed Ω_b. I assume $\Omega_b>0$ with no loss of generality. The bar potential may then be expanded in spherical harmonics:

$$U_b(\mathbf{r}, t)=\sum_{l=2}^{\infty}\sum_{m=-l}^{l}U_{lm}(r)Y_{lm}(\theta,\phi_{rot}), \tag{18}$$

where $\phi_{rot}=\phi-\Omega_b t$. Since the bar is assumed to have a rigid figure, the U_{lm} are independent of time. The $l=0$ term in equation (18) is omitted since it does not contribute to the torque and may be absorbed in the unperturbed galactic potential $U(r)$. The $l=1$ terms vanish by symmetry since the centre of mass of the bar lies at $r=0$.

Since the motion of an unperturbed star is periodic in the canonical coordinates, the bar potential may be expanded in a Fourier series

$$U_b=\sum_{l_3=0}^{\infty}\sum_{l_1,l_2=-\infty}^{\infty}\Psi_{l_1l_2l_3}(I_1,I_2,I_3)\cos(l_1w_1+l_2l_2+l_3w_3-l_3\Omega_b t), \tag{19}$$

where

$$\Psi_{l_1 l_2 l_3}(I_1, I_2, I_3) = \sum_{l=2}^{\infty} \left(\frac{2}{1+\delta_{l_3 0}} \right) V_{l l_2 l_3}(\beta)\, W^{l_1}_{l l_2 l_3}(I_1, I_2), \tag{20}$$

$$V_{l l_2 l_3}(\beta) = r^{l}_{l_2 l_3}(\beta) Y_{l l_2}(\pi/2, 0) i^{l_3 - l_2}, \tag{21}$$

$$W^{l_1}_{l l_2 l_3}(I_1, I_2) = \frac{1}{\pi} \int_0^{\pi} dw_1 \cos[l_1 w_1 - l_2(\psi - w_2)] U_{l l_3}(r), \tag{22}$$

and l_3 is equivalent to the index m of equations (18). In the above expressions, I have employed the summation convention and written $l_p w_p = l_1 w_1 + l_2 w_2 + l_3 w_3$. Since $U_b(\mathbf{r}, t)$ is even in ϕ_{rot}, we have been able to combine the terms with a given l_3 with those for $-l_3$ (see Paper I for details). Thus l_3 goes from 0 to ∞ instead of $-\infty$ to ∞ in equation (19). The angle β is the inclination of the orbital plane to the equatorial plane. I have defined $V_{lnm} = 0$ for $|n| > l$ or $|m| > l$. The $r^{l}_{mn}(\beta)$ are rotation matrices (e.g. Edmonds 1960) which satisfy the orthogonality condition

$$\int_0^{\pi} d\beta \sin\beta\, r^{l}_{mn}(\beta) r^{l'}_{mn}(\beta) = \frac{2}{2l+1} \delta_{ll'} \tag{23}$$

To compute the torque on a single star, I assume $\varepsilon \ll 1$ and solve Hamilton's equations by successive iteration. On the first iteration, the torque on a particle is computed by integrating around the unperturbed trajectory. On the second iteration, the torque is computed by integrating around the first-order perturbed trajectory. To avoid transients caused by suddenly 'turning on' the bar, let $\omega = l_3 \Omega_b + i\eta$, where the small positive parameter η implies $U_b \sim \exp(\eta t)$. This assumption implies that the perturbation was turned on adiabatically in the distant past. Upon averaging over initial phase (with fixed I_j), the first-order contribution vanishes, and the second-order contribution is

$$\langle \Delta_2 \dot{I}_3 \rangle = \frac{1}{2} \eta \exp(2\eta t) \sum l_3 l_k \frac{\partial}{\partial I_k} \frac{|\Psi|^2}{|l_p \Omega_p - l_3 \Omega_b - i\eta|^2}. \tag{24}$$

In the equation above, I have denoted the average of a quantity X over the initial phases of all stars with given momenta I_j by single brackets $\langle X \rangle$. I will also want to consider the integral of a quantity X over all stars in a galaxy. I denote this integral by double brackets:

$$\langle\langle X \rangle\rangle = \int d\mathbf{x}\, d\mathbf{v}\, f(\mathbf{r}, \mathbf{v}) X, \tag{25}$$

where f is the phase-space density.

In equation (24) the torque diverges at the resonances, $l_p \Omega_p - l_3 \Omega_b \to 0$. We have shown in Paper I, however, that if the resonances passes through the orbit rapidly, we can take $\eta \to 0$ and write the divergent factor as a delta function,

$$\delta(x) = \frac{1}{\pi} \lim_{\eta \to 0} \eta |x - i\eta|^{-2}. \tag{26}$$

The integration over the momenta then yields the total torque. For a spherical galaxy, the phase-space distribution function is given by $f = f(I_1, I_2)$. The expression for the total torque on the bar is then

$$\tau_z^{LBK} = -\langle\langle \Delta_2 \dot{I}_3 \rangle\rangle = 4\pi^4 \int_0^{\infty} dI_1 \int_0^{\infty} dI_2 \int_{-I_2}^{I_2} dI_3 \times \sum_{l_3=0}^{\infty} \sum_{l_1, l_2 = -\infty}^{\infty} l_3 l_k \frac{\partial f}{\partial I_k} |\Psi_{l_1 l_2 l_3}|^2 \delta(l_1 \Omega_1 + l_2 \Omega_2 - l_3 \Omega_b). \tag{27}$$

I refer to equation (27) as the LBK torque formula. To this order of approximation, all the contribution to the torque occurs for stars at resonance and the torque is second order in the perturbation Ψ.

I will apply the LBK torque formula to the following model:

(1) The unperturbed system is the singular isothermal stellar sphere discussed in Section 2.

(2) For a bar, one expects the quadrupole terms ($l=2$) to be dominant and thus all higher ($l>2$) terms to the sum in equation (18) are ignored. Assuming U_b to be symmetric about $z=0$, only terms with even $l+m$ exist. Thus, $m=0, \pm 2$. Furthermore, the $m=0$ term may be ignored since it has azimuthal symmetry and thus exerts no torque. The only contributing terms are then $l=2$, $m=\pm 2$. In addition, since U_b is real and even in ϕ_{rot}, it follows that $U_{2,2}=U_{2,-2}$ and all of the U_{lm} are real.

(3) The radial potential, $U_{2,2}(r)$, has the form

$$U_{2,2}(r)=\frac{b_1 r^2}{1+(r/b_2)^5}, \tag{28}$$

where b_1 and b_2 are constants. Thus the potential satisfies Laplace's equation for radii well outside the bar and behaves like the potential of a system with constant density as $r\to 0$. In order to compute the rate of change in pattern speed of the bar due to the torque (see Section 2), the bar must be assigned a mass by fitting equation (28) to a mass model. I discuss one such fit for the homogeneous ellipsoid in Section 3.3.

I now use the properties of the isothermal stellar sphere, equations (5) and (6), to evaluate the orbital parameters given in equations (12)–(17). Since these expressions are functions of E and J and the distribution function is a function of energy only, it is convenient to change interaction variables in equation (27) from (I_1, I_2, I_3) to (E, J, β). In the new variables equation (27) may be written

$$\tau_z^{LBK}=2\pi^4\Omega_b \int\int\int \frac{dE\, dJ^2\, d(\cos\beta)}{\Omega_1} \sum l_3^2 \frac{df}{dE} |\Psi_{l_1 l_2 l_3}|^2 \delta(l_s\Omega_s - l_3\Omega_b). \tag{29}$$

For a given energy, the maximum angular momentum is that of a circular orbit and is given by $J_{max}(E)=\sqrt{2\sigma a_1}\, \exp([\tfrac{1}{2}(E/\sigma^2-1)]$. Now define $\varkappa \equiv J/J_{max}$ and the reduced radius $\tilde{r}=r/a_1 \exp(E/2\sigma^2)$. The reduced turning points $\tilde{r}_p$ and $\tilde{r}_a$ are then given by the roots of the transcendental equation $-2\ln\tilde{r}=\varkappa^2/e\tilde{r}^2$ and are shown in Fig. 1. For circular orbits ($\varkappa=1$), $\tilde{r}_p=\tilde{r}_a=\exp(-\tfrac{1}{2})$ and for radial orbits ($\varkappa=0$), $\tilde{r}_p=0$ and $\tilde{r}_a=1$. The frequencies given by equations (12) and (13) may now be conveniently written as functions of E and $\varkappa$:

$$\Omega_1(E,\varkappa)=\exp(-E/2\sigma^2)\, \nu_1(\varkappa), \tag{30}$$

$$\Omega_2(E,\varkappa)=\exp(-E/2\sigma^2)\, \nu_2(\varkappa), \tag{31}$$

where

$$\nu_1(\varkappa)=\left\{\frac{\alpha_1}{2\pi\sqrt{2\sigma^2}} \int_{C_1} \frac{d\tilde{r}}{[-2\ln\tilde{r}-\varkappa^2/e\tilde{r}^2]^{1/2}}\right\}^{-1}, \tag{32}$$

$$\nu_2(\varkappa)=\frac{\nu_1(\varkappa)\varkappa}{2\pi\exp(\tfrac{1}{2})} \int_{C_1} \frac{d\tilde{r}}{\tilde{r}^2[-2\ln\tilde{r}-\varkappa^2/e\tilde{r}^2]^{1/2}}. \tag{33}$$

The reduced orbital frequencies, ν_1 and ν_2, are shown in Fig. 2 ($\alpha_1=\sigma=1$ in this and all subsequent figures). From epicyclic theory, $\nu_1(\varkappa\to 1)=2\exp(\tfrac{1}{2})$, $\nu_2(\varkappa\to 1)=\sqrt{2}\exp(\tfrac{1}{2})$ and $\nu_2/\nu_1(\varkappa\to 1)=1/\sqrt{2}$. The integral in equation (33) may also be evaluated for $\varkappa\to 0$ yielding $\nu_2/\nu_1(\varkappa\to 0)=1/2$.

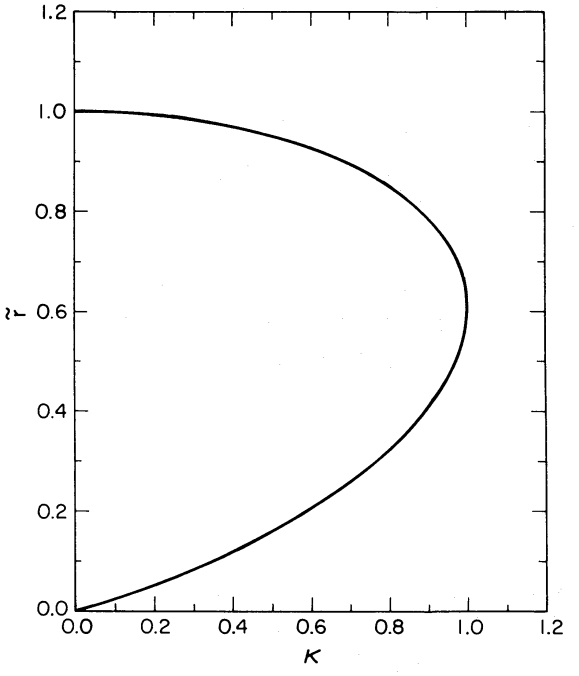

Figure 1. The reduced turning points, $\tilde{r}_p$ and $\tilde{r}_a$, as a function of $\varkappa$.

In order to compute the radial potential transform (equation 22) one also needs to know botl w_1 and the quantity $w_2-\phi$ given by equations (15) and (16) as functions of r (or equivalently $\tilde{r}$) fo a given E and $\varkappa$. These functions are

$$w_1(\tilde{r})=\frac{\nu_1(\varkappa)a_1}{\sqrt{2\sigma^2}}\int_{\tilde{r}_p}^{\tilde{r}}\frac{d\tilde{r}}{[-2\ln\tilde{r}-\varkappa^2/\tilde{r}^2e]^{1/2}}, \tag{34}$$

and

$$f(w_1)=\frac{\nu_2(\varkappa)}{\nu_1(\varkappa)}w_1-\frac{\varkappa}{\exp(\frac{1}{2})}\int_{\tilde{r}_p}^{\tilde{r}}\frac{d\tilde{r}}{\tilde{r}^2[-2\ln\tilde{r}-\varkappa^2/\tilde{r}^2e]^{1/2}}. \tag{3}$$

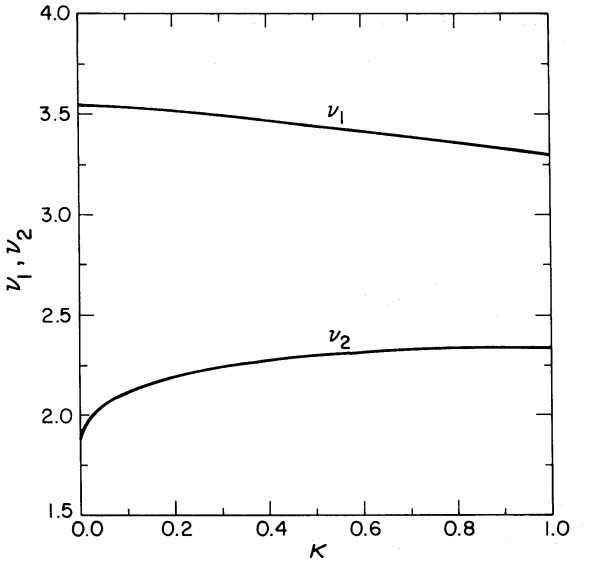

Figure 2. The reduced orbital frequencies, ν_1 and ν_2, in units of σ/a_1 as a function of $\varkappa$.

The resonance condition, $l_1\Omega_1+l_2\Omega_2-l_3\Omega_b=0$, yields a relation between E and $\varkappa$ for a given resonance (l_1, l_2, l_3),

$$E=2\sigma^2\ln\left(\frac{l_1\nu_1(\varkappa)+l_2\nu_2(\varkappa)}{l_3\Omega_b}\right). \tag{36}$$

Since I consider only the $l=2$, $m=\pm2$ components, we have $l_3=2$, and the possible resonances are severely restricted. There are resonances only for $l_3=2$, $l_2=-2, 0, 2$ (see equations 20–22). Using equation (36), the allowed values of l_1 for each of the three l_2 are: (1) $l_2=2$, $l_1=-1, 0, \ldots, \infty$; (2) $l_2=0$, $l_1=1, 2, \ldots, \infty$; and (3) $l_2=-2$, $l_1=2, 3, \ldots, \infty$. In Fig. 3, some of the allowed resonances (l_1, l_2, l_3) are plotted on the $E-\varkappa$ plane. In the limit $\varkappa\to0$ (36) takes the form $E\sim\ln(l_1+l_2/2)+\text{constant}$. Thus, three curves corresponding to $q\equiv l_1+l_2/2$ where $q\in\{1, 2, 3, \ldots\}$ meet at a point at $\varkappa=0$. The resonance $(-1, 2, 2)$ has $q=0$ and thus the energy for a resonant star becomes infinitely negative as $\varkappa\to0$.

The LBK formula (29) may now be greatly simplified. First I use the expression for the bar potential in the canonical variables (19)–(22) together with the orthogonality condition for the rotation matrices (23) to perform the β integration. The integration over energy is also easy. Finally, one is left with the following expression for the torque on the rotating bar by the halo stars:

$$\tau_z^{\mathrm{LBK}}=-\frac{3\pi^3\sigma^2a_1^2f_0}{e\Omega_b}\int_0^1 d\varkappa\,\varkappa\sum_{l_2=-2,0,2}\sum_{l_1=-\infty}^{\infty}[l_1+l_2\nu_2(\varkappa)/\nu_1(\varkappa)]$$
$$\left\{[W^{l_1}_{2\pm22}(E,\varkappa)]^2\,\delta_{l_2\pm2}+\frac{2}{3}[W^{l_1}_{202}(E,\varkappa)]^2\,\delta_{l_20}\right\}. \tag{37}$$

where E is given by equation (36) for the terms in curly brackets. Since $\tau_z^{\mathrm{LBK}}<0$, the bar always

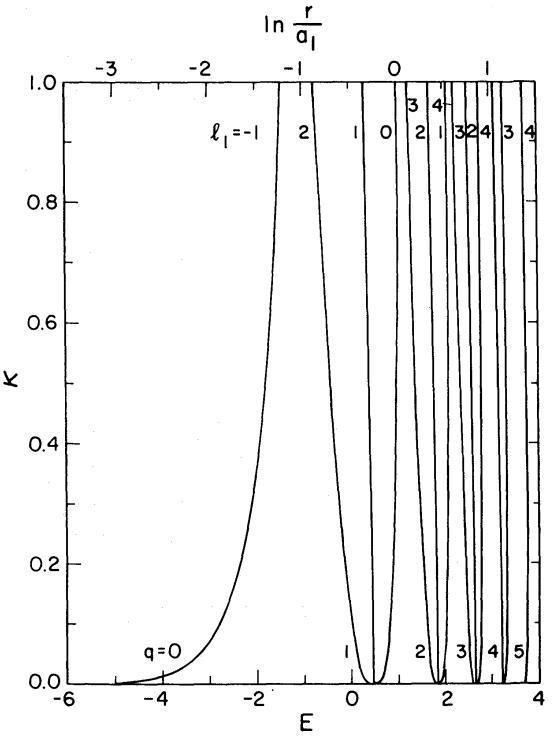

Figure 3. Relationship of E to $\varkappa$ for particular resonances $(l_1, l_2, l_3=2)$ (equation 36). The energy per unit mass, E, is given in units of σ^2. The radii of the circular orbits for resonances are given along the top of the figure and l_1 for each curve is marked. The value of $q=l_1+l_2/2$ for the curves is noted along the $\varkappa=0$ axis.

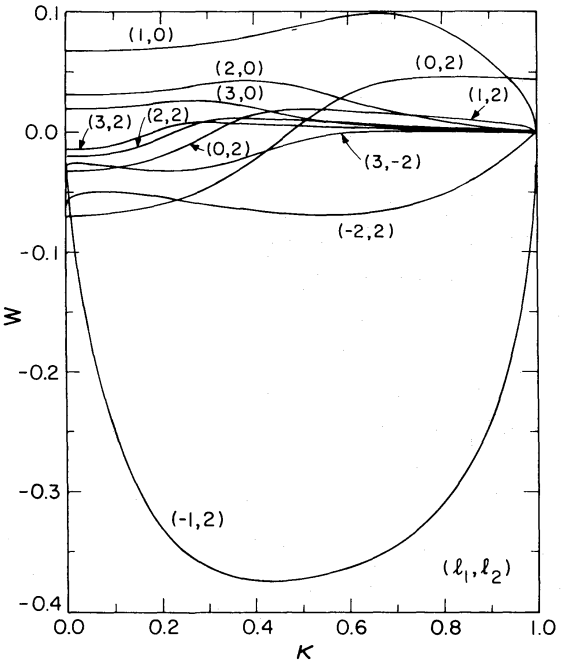

Figure 4. Radial potential transform, $W^{l_1}_{2,l_2,2}$, using the perturbed potential equation (28) with $a_1=b_1=b_2=1$.

loses angular momentum to the halo. Although the sum over l_1 is infinite, only nearly radial orbits contribute to the radial potential transform W for large l_1. In Fig. 4, $W(\varkappa)$ is shown for $l_2=-2, 0, 2$ and $l_1\leqslant 3$. Note that the amplitude drops and that the extrema occur for smaller values of $\varkappa$ as l_1 increases; for increasing radial orbits there is more power in the higher harmonics (*cf.* equation 22). For a similar reason, nearly circular orbits near the $(l_1, l_2, l_3)=(-1, 2, 2)$ resonance will strongly contribute to the total torque. Using Figs 3 and 4 together one may determine the phase–space location of the dominant angular momentum transfer.

I will evaluate equation (37) numerically in Section 3.3. First, however, I will return to the problem of the self-consistency of the LBK formulation and the effects of torques in the limit of slow changes in Ω_b where it does not apply.

3.2 TORQUES IN THE SLOW LIMIT

In Paper I we showed that the validity of the LBK formula (27) depends on a parameter we called the 'speed':

$$s=\left|\frac{l_3\dot{\Omega}_b}{\Psi_{l_1l_2l_3}l_k\partial l_p\Omega_p/\partial I_k}\right|. \tag{38}$$

If $s\gg 1$ the LBK formula is recovered and if $s<1$ slow limit effects dominate. For strong bars, the slow-limit contribution to the total torque will be shown to be negligible. Thus, the reader who is interested mainly in results may skip to Section 3.3. In the remainder of the subsection, I will discuss the expression for the torque on the bar in the slow limit and discuss the possibility that stars may be captured into resonance with the bar.

In the slow limit $s<1$, we found (Paper I) the following expression for the torque to lowest order in $\varepsilon^{1/2}$:

$$\tau_z^{NL}=(2\pi)^3\int_0^\infty dI_1\int_0^\infty dI_2\int_{-I_2}^{I_2}dI_3 f(I_j)$$
$$\times\sum_{l_3=0}^{\infty}\sum_{l_1,l_2=-\infty}^{\infty} l_3\dot{\Omega}_b\,|\Psi_{l_1l_2l_3}|^{1/2}\frac{\mathrm{sgn}(l_k\partial l_p\Omega_p/\partial I_k)}{|l_k\partial l_p\Omega_p/\partial I_k|^{1/2}}Q(s)\delta(l_s\Omega_s-l_3\Omega_b), \tag{39}$$

where s is given by equation (38) and $Q(s)$ is a monotonic decreasing function with $Q(s=0)=8/\pi$ and $Q(s\geq 1)=0$. The function $Q(s)$ is given by

$$Q(s)=\frac{\sqrt{2}}{\pi s}\int_{z_1}^{z_2} dx \sin x[\cos x_1-\cos x+s(x_1-x)]^{1/2}, \qquad x_1=\sin^{-1}s, \qquad 0<x_1<\pi/2, \tag{40}$$

and x_2 is the first root of the radicand which exceeds x_1. In contrast to dynamical friction, the momentum changes in the slow limit are reversible: that is, the sign of the torque depends on the sign of $\dot{\Omega}_b$. Thus, for example, if a bar is artificially slowed and then speeded up, so that a resonance passes twice through an ensemble of stars, then the net angular momentum transfer will be zero to $O(\varepsilon^{1/2})$. Thus, these interactions cannot be considered to be dynamical friction; a more appropriate name might be 'dynamical feedback.' Using the definitions in Section 3.1, equation (39) may be rewritten in the variables E and $\varkappa$:

$$\tau_z^{NL}=16\pi^3\sigma^4 f_0 a_1^2\frac{1}{e}\frac{\dot{\Omega}_b}{\Omega_b^2}\int_0^{\pi} d\beta \sin\beta \int_0^1 \frac{d\varkappa\,\varkappa}{\nu_1(\varkappa)}$$
$$\times\sum_{l_2=-2,0,2}\sum_{l_1=-\infty}^{\infty}[l_1\nu_1(\varkappa)+l_2\nu_2(\varkappa)]|\Psi_{l_1l_2l_3}|^{1/2}\frac{\operatorname{sgn}(l_k\partial l_p\Omega_p/\partial I_k)}{|l_k\partial l_p\Omega_p/\partial I_k|^{1/2}}Q(s). \tag{41}$$

Since s depends on the inclination β through the potential Ψ, one cannot integrate analytically over β as in the case of the LBK formula.

I will now make the approximation that for $s<1$ the torque is given by equation (41) and for $s>1$ the torque is given by the LBK formula (27). I have ignored the details of the transition region $s\sim 1$ in making this assumption, but numerical calculations indicate that the LBK formula is only significantly in error for $1<s\lesssim 2$. Since there is no reason to expect a large fraction of the resonances to have $s\sim 1$, the details around $s\sim 1$ will probably not be qualitatively significant. The total torque is the sum of the contributions from the LBK and the slow regimes

$$\tau_z^{total}=I\dot{\Omega}_b=\tau_z^{LBK}+\tau_z^{NL}. \tag{42}$$

Since τ_z^{NL} is proportional to $\dot{\Omega}_b$, we define $(dJ_b/d\Omega_b)^{NL}\equiv\tau^{NL}/\dot{\Omega}_b$ where $J_b=I\Omega_b$ is the angular momentum of the bar. Employing equation (42) gives

$$\dot{\Omega}_b=\frac{\tau_z^{LBK}}{I-(dJ_b/d\Omega_b)^{NL}}. \tag{43}$$

Note that if all angular momentum transfer were to occur in the slow limit, $\tau_z^{LBK}=0$ leading to $\dot{\Omega}_b=0$. This is a consequence of the reversibility of dynamical feedback. In practice, equation (43) must be solved by iteration since $(dJ_b/d\Omega_b)^{NL}$ depends on $\dot{\Omega}_b$ through s. This will be done in Section 3.3.

Another possible outcome of a star passing through resonance in the non-linear regime is capture into libration about the rotating bar. Capture must be studied by analysis of the equations of motion for a single star in the bar–halo system since the averaging procedure used in deriving equation (39) destroys the phase-space topology that leads to capture (Lichtenberg & Lieberman 1983, p. 65). We performed such an analysis in Paper I and showed that in the LBK regime ($s>1$) the capture probability is zero, and for very slow transitions ($s\ll 1$) the capture probability is of order $\varepsilon^{1/2}$. Motivated by observations of barred galaxies, in this paper I assume the bar is strong and ends at corotation for which nearly all resonances are in the fast limit as I will demonstrate in the following subsection.[1] Since captures are not important for the models presented, I will not discuss their consequences further in this paper.

[1]If, however, the bar is weak or slowly rotating, a non-negligible fraction of stars may be in the slow limit. As discussed in Paper I, the bar may then acquire a cloud of captured stars of order $\varepsilon^{1/2}$, which may be much larger than the original bar mass which is of order ε. The effect of captured stars is to increase the effective moment of inertia of the bar since any change in pattern speed requires angular momentum transfer to the captured stars (see equation 8 and following discussion).

3.3 NUMERICAL RESULTS

I will now evaluate equations (37) and (43) numerically and derive the 'slow-down time' for a bar. I define the slow-down time to be

$$T_{\rm slow}=-J_{\rm b}/\dot{J}_{\rm b}=-\Omega_{\rm b}/\dot{\Omega}_{\rm b}, \tag{44}$$

where $\Omega_{\rm b}$ is initial pattern speed and the second equality follows from the assumption that the bar rotates as a solid body (see Section 2). The quantity $T_{\rm slow}$ is the instantaneous e-folding time for pattern-speed decay. Note that this time differs from the half-life, $T_{1/2}$, defined in Section 1 although it is of the same order. The number of initial rotation times for a given slow-down is then given by

$$N=T_{\rm slow}/T_0=T_{\rm slow}\Omega_{\rm b}/2\pi. \tag{45}$$

In order to evaluate equation (45), a moment of inertia for the bar model must be chosen since we have discarded the $m=0$ terms which contribute to the moment of inertia. To choose the mass model, I will fit the perturbed bar potential equation (28) to the exact $Y_{2,\pm2}$ component of the potential of a homogeneous ellipsoid with principal axes $a_1>a_2>a_3$. The parameters b_1 and b_2 are chosen to match the exact component as $r\to0$ and $r\to\infty$:

$$b_1=\pi G\varrho\sqrt{\frac{2\pi}{15}}(A_1-A_2), \tag{46}$$

$$b_2^5=\frac{2}{5}a_1a_2a_3\frac{a_2^2-a_1^2}{A_1-A_2}, \tag{47}$$

where

$$A_i=a_1a_2a_3\int_0^\infty du/(a_i^2+u)\sqrt{(a_1^2+u)(a_2^2+u)(a_3^2+u)}$$

(Chandrasekhar 1969). The mass of the bar is defined to be a fixed fraction, $\mu_{\rm b}$, of the mass of the stellar component inside the bar radius (*cf.* equation 6)

$$M_{\rm b}=\frac{2\sigma^2a_1}{G}\mu_{\rm b}, \tag{48}$$

and therefore the moment of inertia of the bar rotation about the a_3 axis is

$$I=\frac{2\sigma^2a_1}{5G}\mu_{\rm b}(a_1^2+a_2^2). \tag{49}$$

Table 1. LBK formula.

b_2'	$\tilde{\tau}$
0.25	7.64×10^{-5}
0.50	1.66×10^{-2}
0.75	3.04×10^{-1}
1.00	1.53
1.25	3.80
1.50	7.78
1.75	16.9
2.00	37.7
2.50	156
3.00	460

As in Section 1 the corotation parameter may be defined:

$$S=\Omega_b a_1/\sqrt{2}\sigma. \tag{50}$$

Thus, $S>1$ ($S<1$) if the end of the bar is outside (inside) corotation. If a_1 and σ are fixed then Ω_b is determined by S.

Now, to evaluate the LBK formula for the model potential (28), note that up to a multiplicative factor the expression (37) depends only the parameter $b_2 S/a_1$. Thus, it is convenient to define the dimensionless torque

$$\tilde{\tau}=-\tau_z^{\rm LBK}(b_2'=2\sqrt{2}Sb_2/a_1, a_1=\sigma=\Omega_b=f_0=1), \qquad \tilde{U}_b(r)=r^2/[1+(r/b_2')^5]. \tag{51}$$

In evaluating equation (51), I use $\tilde{U}_b(r)$ instead of $U_b(r)$ in the LBK formula (37). Equation (37) may then be written

$$\tau_z^{\rm LBK}=-\frac{b_1^2 a_1^6 \sigma^2 f_0}{128 S^4 \Omega_b}\tilde{\tau}. \tag{52}$$

Thus, one only needs to determine a one-parameter family $\tilde{\tau}(b_2')$ to determine $\tau_z^{\rm LBK}$ for this model. The function $\tilde{\tau}(b_2')$ has been tabulated as a function of b_2' in Table 1. Note that the torque drops rapidly for $S\ll 1$ since the strongest resonances lie well outside the bar.

Using equations (45), (46), (50), and (52) one obtains an expression for the number of rotation times for slow down

$$N=\frac{2^{12}\pi^{1/2}}{3}\frac{(1+\alpha^2)\alpha^2\beta^2}{(A_1-A_2)^2\mu_b}\frac{S^7}{\tilde{\tau}}, \tag{53}$$

where $\alpha\equiv a_2/a_1$ and $\beta\equiv a_3/a_1$. I will call the model with $\alpha=0.2$, $\beta=0.1$, and $\mu_b=1$ the 'standard model'. These parameters were all suggested by Kormendy (1983, private communication) as typical parameters of observed bars. The standard bar with $S=1$ slows down in $N=0.965$ initial bar rotation times. If the standard bar has $S=1.5$ it slows in 2.7 initial rotation times; for $S=1/2$ it

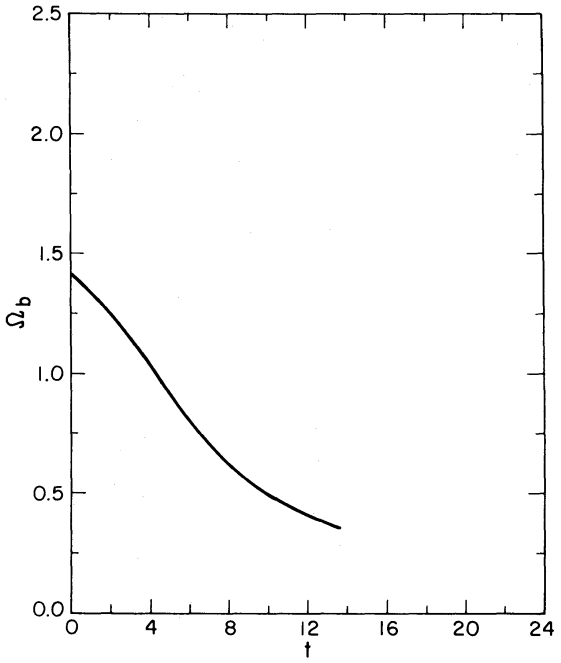

Figure 5. Pattern speed as a function of time for the standard model. The pattern speed is given in units of σ/a_1 and the time is in units of a_1/σ.

slows in 0.39 initial rotation times. A better estimate may be obtained by integrating equation (52) in time assuming that the bar is rigid. In Fig. 5, the resulting pattern speed is plotted as a function of time for $S=1$. The maximum rate of slow down occurs at 0.3 rotation times where $S\simeq 0.7$. For the standard model $T_{1/2}\simeq 1.6\,T_0$. I conclude that the bar slows significantly in several rotation times. Since these results were derived using perturbation theory, the extrapolation to $\mu_b=1$ is not strictly justified; however the n-body simulations described in Section 4 substantiate these results.

As I mentioned in Section 2, the isothermal sphere does not rotate. The possibility remains that a rotating halo could significantly change the rate of angular momentum transfer to the bar. To investigate this possibility, the isothermal sphere may be simply modified to produce a family of rotating halo models. Since at any point in the isothermal sphere the distribution function (equation 7) only depends on the magnitude of the velocity, any star may be reversed in its orbit without changing the density of the halo. In terms of the variables of equation (29), this transformation corresponds to $(E, J, \beta)\rightarrow(E, J, \pi-\beta)$. By reversing a fraction of the retrograde orbits, say those with $\pi/2(2-x)\leqslant\beta\leqslant\pi$ where $0\leqslant x\leqslant 1$, one may construct a family of rotating haloes and study their effect on the bar slow-down rate. Since the density of these rotating models is the same as that of the isothermal sphere, the LBK torque formula (equation 27) is still valid and may be used with an appropriate modified distribution function to compute the torque on the bar as a function of x. Performing the computation, I find that the rate at which the bar loses angular momentum *increases* monotonically as x varies from 0 to 1. In the extreme case of no retrograde orbits at all, $x=1$, the torque is a factor of 1.46 larger than that for the standard model. The reason for this increase is that prograde orbits have a stronger effect on the bar than retrograde orbits. More specifically, one can show from equation (21) that prograde (retrograde) orbits contribute predominantly to the $l_2=2$ ($l_2=-2$) resonances and both prograde and retrograde orbits contribute equally to the $l_2=0$ resonances. Since the $l_2=2$ resonances are generally stronger than the $l_2=-2$ resonances (see Fig. 4) for a given l_1, increasing the number of prograde orbits at the expense of retrograde orbits increases the torque on the bar.* In summary, the dynamical slow down of a bar in a rotating halo is not significantly different from the slow down for the standard model presented above.

I now will discuss the effect of slow-limit torques on the bar slow-down time. Since the integrand of $(dJ_b/d\Omega_b)^{NL}$ depends on μ_b the right-hand side of equation (41) can not be evaluated as a simple one-parameter family. Instead, I will calculate N by using equation (43) for the parameters of the standard model with $S=1$ but varying μ_b (see Table 2). For the true standard model ($\mu_b=1$) one finds that the slow limit is unimportant and the value for N is the same as

Table 2. Non-linear slow down.

μ_b	N	$(dJ_b/d\Omega_b)^{NL}/I$
0.01	1492	-14.5
0.02	200	-3.16
0.03	49.4	-5.36×10^{-1}
0.05	19.8	-2.67×10^{-2}
0.10	9.65	1.02×10^{-2}
0.20	4.81	7.41×10^{-4}
0.40	2.41	2.67×10^{-5}
0.60	1.61	8.94×10^{-8}
0.80	1.21	2.00×10^{-8}
1.00	0.965	3.84×10^{-9}

*There is an additional contribution due to the discontinuity of the modified distribution in I_3 which tends to decrease the torque but it is small compared with the effect just described.

quoted above. Only eccentric orbits ($\varkappa \ll 1$) in the strongest resonance $(l_1, l_2, l_3) = -(-1, 2, 2)$ (*cf.* Fig. 4) interact with the bar in the slow limit. These orbits transfer angular momentum from the bar to the halo. As μ_b decreases, more and more orbits contribute to the slow-limit torque and N falls below the LBK value but the differences are small for $\mu_b \gtrsim 0.1$. For $\mu_b \lesssim 0.05$, weaker resonances also contribute to the slow limit. The weaker resonances exert torques in the opposite sense: angular momentum is transferred from the stars to the bar. This results in $(dJ_b/d\Omega_b)^{NL}/I$ becoming negative and N becoming larger than the LBK values. For $\mu_b = 0.05$ N is 3 per cent larger than the LBK value, and for $\mu_b = 0.03$ it is 54 per cent larger. Alternatively, we may consider the effect of slow-limit torques for the standard model ($\mu_b = 1$) and variable S. If $S \ll 1$, we have seen that Ω_b from the LBK formula will be small and the slow limit will be important (*cf.* equation 38). Therefore, decreasing S will lead to similar behaviour as decreasing μ_b. Thus, torques in the slow limit may be important for the evolution of both weak or slowly rotating bars.

As was noted in Section 3.2, the theory does not include capture into resonance which would stabilize the slow down by increasing the effective moment of inertia.

3.4 DISC TORQUES

So far, I have only considered the angular momentum transfer between the bar and the halo, but the rotating bar will also interact with the disc. If the disc accepts angular momentum from the bar, the presence of the disc will tend to reinforce angular momentum transfer from the bar to the halo demonstrated in the previous subsection. However, if the disc deposits angular momentum in the bar one might expect a steady state to be reached in which the torque of the disc on the bar equals the torque of the bar on the halo. In this case, the bar acts as a catalyst, enabling the disc to shed its angular momentum and achieve a lower energy state.

Just as the bar induces a wake in the halo which exerts a torque on the bar, the bar may excite density waves in the disc which may transfer angular momentum to the bar. Goldreich & Tremaine (1979) investigated the excitation of density waves at the Lindblad and corotation resonances in a gas disc by an external potential and determined the angular momentum transfer rate. They showed that the results also apply to a stellar disc and in the epicyclic limit ($\varkappa \to 1$) reduce to the LBK formula in two dimensions (which is the form originally derived by Lynden-Bell & Kalnajs 1972). The expression can be used to determine the torques between the bar and the disc. Let the external perturbation be a rotating bar and assume the background disc is such that the excitation of density waves cause a positive torque on the bar, τ_z^{DISC}. Then, equating the bar–halo torque to the bar–disc torque, $\tau_z^{DISC} = \tau_z^{LBK}$, gives an implicit relationship for the equilibrium pattern speed and disc parameters. To derive this relationship, I choose an unperturbed disc with the density $\Sigma(r) = \Sigma_0 r_0/r$ which has a logarithmic potential. I parametrize the 'strength' of the disc by defining the quantity γ to be the ratio of the radial force at r due to the disc component to the radial force due to the isothermal halo. Thus, $\gamma = \pi G \Sigma_0 r_0/\sigma^2$ which is, coincidentally, also equal to the ratio of the mass of the disc to the mass of the halo inside radius r.

Table 3. Bar–halo–disc steady state.

S	γ
0.25	4.0
0.50	0.52
0.75	0.029
1.00	0.023
1.25	0.038
1.50	0.091

One finds that angular momentum is deposited in the bar by the inner Lindblad resonance and accepted by the disc at the outer Lindblad resonance while the corotation resonance does not contribute at all. The inner Lindblad resonance dominates the contribution over all parameters of interest. The steady-state values of the disc ratio γ as a function of corotation parameter for the standard bar model are shown in Table 3.

Since we expect $\gamma \sim 1$, the end of the bar is inside corotation, $S \lesssim 0.5$, for steady-state. This result, however, is likely to be strongly dependent on the disc model. The most important conclusion to be drawn from this model is the possibility that the bar–halo–disc interaction may yield a steady pattern speed. Note that the steady-state scenario depends on the existence of an inner Lindblad resonance between the bar and the disc; if there is no inner Lindblad resonance, the disc would accept angular momentum at the outer Lindblad resonance and no steady state would be possible. Sellwood (1981) found that in his models, bars tend to avoid the inner Lindblad resonance. Sanders & Tubbs (1980), on the other hand, conclude that in order to produce realistic gas dynamics there must be a least one inner Lindblad resonance within the bar. It is not clear whether or not galactic bars have inner Lindblad resonances in general.

4 Numerical simulation

N-body simulations can be used to test a number of the approximations used in the previous sections. The most important are: (1) the restriction of the bar potential used in Section 3 to only the Y_{22} component; and (2) the use of perturbation theory which is only strictly valid for $\mu_b \ll 1$ while observed bars have $\mu_b \sim 1$.

In the same spirit as the analytic dynamical friction calculation, I again assume the stars only respond to the force derived from the unperturbed potential and the bar potential and ignore star–star interactions. Lin & Tremaine (1983) have called this approach the 'semi-restricted' *n*-body technique. There are two principal advantages of this approach over a full *n*-body simulation: (1) the computational complexity scales only as n rather than n^2 which is a great savings in CPU time for large n; and (2) the neglect of the star–star interactions is consistent with the perturbation theory in Section 3 which is what we are trying to check.

4.1 METHOD

The simulation requires the simultaneous solution of $6n+2$ first-order ODE's where n is the number of stars. The two additional equations describe the evolution of the rigid bar. The bar is assumed to rotate about a fixed (z) axis.

Motivated by the perturbation theory, I choose the initial distribution of stars to cover phase space around the dominant lowest-order resonances assuming that the $Y_{2,\pm 2}$ component of the potential is dominant. Since the terms with $l>2$ will also contribute to the torque and the widths of the resonances in the E–$\varkappa$ plane will be broadened by the changing pattern speed, the precise identification of individual resonance is not strictly valid but is only heuristically useful. The locations of the $l=2$, $m=\pm 2$ resonances can be roughly estimated from Fig. 3. For all resonances indices except $(l_1, l_2)=(-1, 2)$ a given resonance has only a slight variation of E as a function of $\varkappa$. Thus, I distribute the stars using a Monte-Carlo procedure according to equation (6) but only with $E_{\min} \leqslant E \leqslant E_{\max}$. Since there is a constraint on the number of stars that can be included in a simulation, the range $[E_{\min}, E_{\max}]$ must be chosen carefully, subject to two constraints: (1) it must cover the main resonances over the course of the evolution; and (2) it must be chosen small enough such that there are always enough stars in the resonances so that the first-order terms average to zero.

The quantity μ_s is defined to be the ratio of the mass of a star to the mass of the distribution inside the bar radius. The $6n+2$ equations of motion then become:

$$\frac{d\mathbf{r}_i}{dt}=\mathbf{v}_i \tag{54}$$

$$\frac{d\mathbf{v}_i}{dt}=-\frac{2\sigma^2}{r_i^2}\mathbf{r}_i-\nabla U_b(\mathbf{r}_i, t) \tag{55}$$

$$\frac{d\phi}{dt}=\Omega_b \tag{56}$$

$$\frac{d\Omega_b}{dt}=-\frac{5\mu_s}{(a_1^2+a_2^2)\mu_b}\sum_{i=1}^{n}\left(x_i\frac{dv_i}{dt}-y_i\frac{dv_i}{dt}\right). \tag{57}$$

After a sufficiently long time, the bar may achieve equipartition with the halo stars at which point further net angular momentum transfer will cease. This equipartition is a numerical artifact resulting from small n approximation and will limit the validity of the simulations for large t; of course, for a real galaxy $\Omega_{b;eq}$ would be negligible. The condition for equipartition may be written:

$$\frac{1}{2}I_b\Omega_{b;eq}^2\simeq\frac{1}{2}m_s\sigma^2, \tag{58}$$

where m_s is the mass of a halo star. For the ellipsoidal bar with n halo stars and a given energy range, the above condition gives an equipartition value for the pattern speed:

$$\Omega_{b;eq}^2\simeq 5\frac{\mu_s}{\mu_b(1+\alpha^2)}. \tag{59}$$

Note that too small a value of μ_b may result in equipartition of energy between the individual stars and the bar at an unacceptably large pattern speed. For this reason and since I am primarily interested in checking the validity of the slow down times obtained in Section 3 I choose $\mu_b=1$ for the simulations below.

In all the simulations I choose $\alpha_1=\sigma=1$ so that $\Omega_b=\sqrt{2}S$ initially and thus an initial rotation time, T_0, is $\sqrt{2}\pi/S$ time units.

4.2 RESULTS

I again use the parameters of the standard model ($\alpha=0.2, \beta=0.1, \mu_b=1.0$) given in Section 3.3 and take $n=1000$ to define a standard simulation using the homogeneous ellipsoidal bar. Notice that in the standard simulation, the ellipsoidal bar exerts a net radial force on a star in addition to that from the isothermal halo and therefore corotation is beyond the end of the bar for $S=1$. To account for this, I define $S=\sqrt{2}$ in the standard simulation so that a star in a circular orbit at $r=a_1$ would be in corotation if $\alpha=\beta=\mu_b=1$. After some experimentation, I found that the slow down in the standard simulation was smooth for the energy range $[-6, 2]$.

In Fig. 6, I show three runs of the standard simulation ($S=\sqrt{2}$) to give an indication of the statistical error in the model. In Fig. 7, I show three runs with $S=1$ to investigate the sensitivity of the evolution to the corotation parameter. In both cases $T_{1/2}\simeq 3.5\,T_0$ demonstrating that standard simulation is not sensitive to the exact position of corotation. However, the half-life is a factor of 2.2 greater that the analytic estimate in Section 3. A possible source of this discrepancy is the

additional radial force from the ellipsoidal bar. Since the velocities of the background stars are initially in an isothermal distribution, the addition of the massive bar systematically decreases $\varkappa$ for most orbits and thus decreases the strength of the primary resonances which have their main contribution from nearly circular orbits (see Fig. 4 and equation 37). In Section 3, I was able to avoid this complication by ignoring the axisymmetric terms in equation (18). To investigate this problem, I ran one simulation with $S=\sqrt{2}$ and one with $S=1$ but with the initial velocities of the stars increased by a factor of $\sqrt{2}$. The simulations give $T_{1/2}\simeq 1.8\,T_0$, $1.1\,T_0$, for $S=\sqrt{2}$, 1. This is in closer agreement with the perturbation theory result: $T_{1/2}\simeq 1.6\,T_0$. Thus, it seems that the distortion of the unperturbed potential by the bar does slow the evolution.

For the standard model the equipartition pattern speed given by equation (59) is $\Omega_{b;eq}\simeq 0.12$. From Figs 6 and 7, we see that the pattern speed has levelled off by $t=24$ to $\Omega_b\simeq 0.5$ which is above the equipartition value. In fact from previous arguments, there are several reasons why the actual limiting pattern speed may be above $\Omega_{b;eq}$. First, as Ω_b becomes smaller, the resonant stars will have higher values of energy and since the energy range is limited, only a small subset of the population will be involved in angular momentum transfer. Secondly, if the resonances involved are sparsely populated, angular momentum transfer will be inefficient before the equipartition limit is reached. Thirdly, the angular momentum transfer rate decreases as Ω_b decreases so that the rate at which equipartition is approached decreases.

Since the bar is turned on suddenly in the equilibrium isothermal sphere, one might worry that the expected evolution may be obscured by transients. To investigate the effect of transients, I let the system evolve for a fraction p of an initial rotation time with the pattern fixed to its initial value so that the stars are forced by the bar but the bar does not react. During this time the bar mass is gradually increased to its true value according to the rule $\mu(t)=\mu_b \sin^2(\pi t/2pT_0)$. This procedure is analogous to the adiabatic turn-on that was employed in the perturbation theory. However, the angular momentum added by the bar during the turn-on phase modifies the equilibrium stellar distribution, and if p is large, the distribution will be significantly distorted by the time the bar is

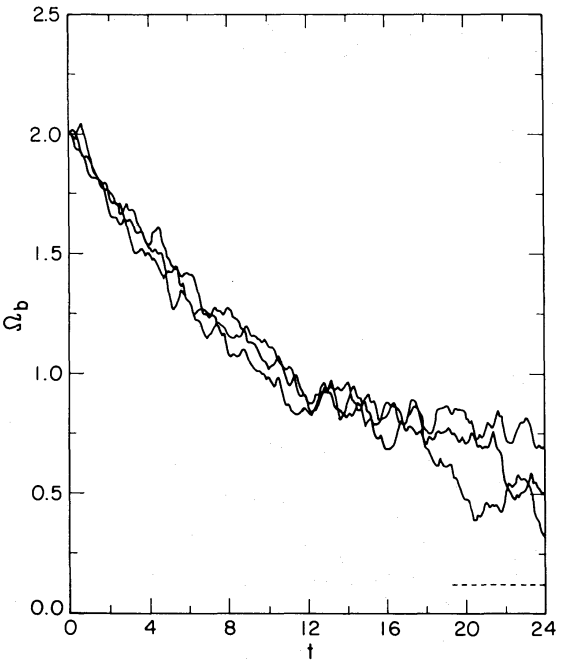

Figure 6. Three runs of the standard simulation: number of stars $n=1000$, corotation parameter $S=\sqrt{2}$, axis ratios $\alpha=0.2$ and $\beta=0.1$, bar mass ratio $\mu_b=1.0$ and energy range $[E_{min}, E_{max}]=[-6, 2]$. The equipartition speed, $\Omega_{b;eq}$, is marked by a dashed line.

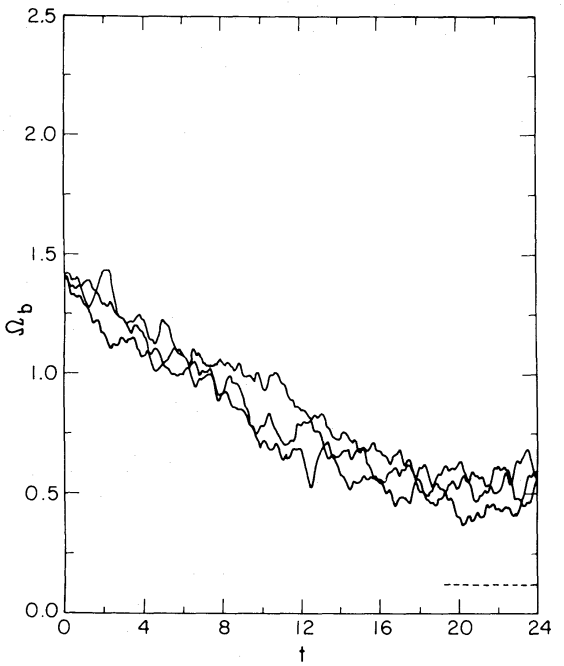

Figure 7. Three runs of the standard simulation but with $S=1.0$.

allowed to interact. I found that runs with $p\leqslant 0.5$ were not substantially affected by this procedure. For $p=1$ the evolution was slightly slower and noisier, possibly because the turn-on was so slow that few stars are left near resonance once the bar is allowed to react. Nevertheless, if there were significant transients, one would expect a noticeable difference between the runs with $p=0.0$ and $p=0.5$. Since the difference between these two runs was negligible, I conclude that initial transients are unimportant in the standard simulation.

As a further comparison between the simulation and the analytic results, I attempted to reproduce the results of the perturbation theory in Section 3 by using the model radial potential equation (28) and the parameters of the standard bar model from equations (46) and (47) instead of the homogeneous ellipsoid. Although one would really like to take $\mu_b \ll 1$ as required by the perturbation theory, the simulation is limited by spurious equipartition and again I take $\mu_b=1$. For these simulations I found that the range $[-2.5, 2]$ gave smooth evolution for $n=500$. I also found minor transient increases in pattern speed which could be damped by taking $p=0.1$. I now compare the numerical simulations with the analytic results of Section 3. The pattern speed curves for this model are shown in Fig. 8 for three cases. For these simulations $T_{1/2}\simeq 0.4\,T_0$ which is approximately a factor of 4 smaller than the analytic prediction. Thus, the angular momentum transfer occurs at a larger rate in the simulations than in the perturbation theory. Although this discrepancy is disturbing, the main purpose of this investigation is to show that $T_{1/2}\sim T_0$, which these simulations demonstrate.

It is interesting to compare the results obtained here to those of Sellwood's live halo simulation (Sellwood 1980). Sellwood began with a relaxed halo component to which he added a disc of equal mass. He found that most of the disc component form a bar which ends at corotation. By following the angular momentum in each component, Sellwood found that the bar also transfers angular momentum to the halo component. Sellwood's run 106 gives $T_{\rm slow}\simeq 5\,T_0$ which may be compared to the standard simulation which gives $T_{\rm slow}\simeq 4.5\,T_0$. Given the inherent differences the two models, such as different bar geometry and central concentration of the halo, the two rates of angular momentum transfer are qualitatively the same.

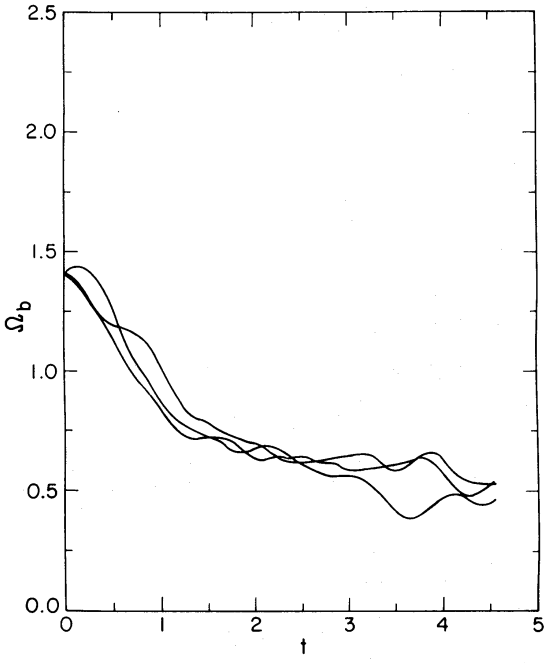

Figure 8. Three simulations using the standard bar model in Section 3.3 with number of stars $n=500$, corotation parameter $S=1.0$, initial growth period $p=0.1$, and bar mass ratio $\mu_b=1.0$.

To summarize the numerical results, it was found that: (1) The rate of angular momentum transfer in the simulations is larger than the predictions of the perturbation theory for the same bar potential (equation 28). This suggests that the LBK formula may underestimate the torque when μ_b is large; (2) using a homogeneous ellipsoid as a bar model instead of only the $l=2$, $m=2$ component we find $T_{1/2}\simeq 3.5\,T_0$. Although this is a larger half-life than that predicted by the analytic theory, it is still significantly smaller than a galactic lifetime.

5 Conclusions

I have computed the angular momentum transfer between a bar and a spherical halo using both analytic perturbation theory and numerical simulations. If the end of the bar is initially at corotation, a strong bar may transfer a significant fraction of its angular momentum to the halo component in a few rotation times. If bars rotate more slowly ($S\ll 1$), are weak ($\mu_b\ll 1$), or if the halo component is significantly more centrally condensed than the isothermal sphere, the slow-down time may be considerably longer. However, simulations of gas forcing by bars (Sanders & Tubbs 1980) suggest that bars do end in the vicinity of corotation (also see Contopoulos 1980), photometric observations show that strong bars are common, and their flat rotation curves indicate that they may indeed have extended massive halos (Kormendy 1983). The rapid angular momentum transfer found in these calculations suggests two possible scenarios. First, bars may gain angular momentum, possibly from the disc at the inner Lindblad resonance. Secondly, the method of angular momentum transfer discussed here may be suppressed, for example, if the halo has been cleared out of the region around the bar. In order to proceed further, the self-consistent responses of the bar and halo to the torques will have to be considered. Our results suggest that it would be worthwhile to carry out long-term N-body calculations of the evolution of discs in live halos.

We see that the simplest model for the interaction between a galactic bar and massive halo by dynamical friction leads to significant transfer of the bar's angular momentum to the halo in much

less than a Hubble time. The rapid angular momentum transfer predicted by this model places strong constraints on our picture of barred galaxy evolution.

Acknowledgments

It is a pleasure to thank Scott Tremaine for his advice and encouragement while this work was in progress. I also thank Alar Toomre for useful discussions. This research was supported in part by National Science Foundation grant AST-8307654.

References

Chandrasekhar, S., 1943. *Astrophys. J.,* **97,** 257.
Chandrasekhar, S., 1969. *Ellipsoidal Figures of Equilibrium.* Yale University Press, New Haven.
Combes, F. & Sanders, R. H., 1981. *Astr. Astrophys.,* **96,** 164.
Contopoulos, G., 1980. *Astr. Astrophys.,* **81,** 198.
Edmonds, A. R., 1960. *Angular Momentum in Quantum Mechanics,* Princeton University Press, Princeton.
Goldreich, P. & Tremaine, S., 1970. *Astrophys. J.,* **233,** 857.
Hohl, F., 1976. *Astron. J.,* **81,** 30.
Hohl, F., 1978. *Astron. J.,* **83,** 768.
Kalnajs, A., 1972. In: *Gravitational N-body Problem,* ed. Lecar, M., Reidel, Dordrecht, Holland.
Kormendy, J., 1982. *Astrophys. J.,* **257,** 75.
Kormendy, J., 1983. *Astrophys. J.,* **275,** 527.
Lichtenberg, A. J. & Lieberman, M. A., 1983. *Regular and Stochastic Motion,* Springer-Verlag, New York.
Lin, D. N. C. & Tremaine, S., 1983. *Astrophys. J.,* **264,** 364.
Lynden-Bell, D., 1979. *Mon. Not. R. astr. Soc.,* **187,** 101.
Lynden-Bell, D. & Kalnajs, A., 1972. *Mon. Not. R. astr. Soc.,* **157,** 1.
Mark, J. W.-K., 1976. *Astrophys. J.,* **206,** 418.
Miller, R. H., 1978. *Astrophys. J.,* **223,** 811.
Miller, R. H. & Smith, B. F., 1979. *Astrophys. J.,* **227,** 785.
Ostriker, J. P. & Peebles, P. J. E., 1973. *Astrophys. J.,* **186,** 467.
Sandage, A. & Tammann, G. A., 1981. *A Revised Shapley–Ames Catalog of Bright Galaxies,* Carnegie Institute of Washington, Washington, DC.
Sanders, R. H. & Tubbs, A. D., 1980. *Astrophys. J.,* **235,** 803.
Sellwood, J. A., 1980. *Astr. Astrophys.,* **89,** 296.
Sellwood, J. A., 1981. *Astr. Astrophys.,* **99,** 362.
Tremaine, S. & Weinberg, M. D., 1984. *Mon. Not. R. astr. Soc.,* (Paper I), **209,** 729.
Weinberg, M. D. & Tremaine, S., 1983. *Astrophys. J.,* **264,** 364.
White, S. D. M., 1983. *Astrophys. J.,* **274,** 53.